



Octupolar ordering of classical kagome antiferromagnets in two and three dimensions

M. E. Zhitomirsky

DSM/INAC/SPSMS, Commissariat à l'Energie Atomique, 17 rue des Martyrs, F-38054 Grenoble, France

(Received 7 May 2008; revised manuscript received 8 August 2008; published 29 September 2008)

Classical Heisenberg antiferromagnets on two-dimensional kagome and three-dimensional hyperkagome lattices are investigated by Monte Carlo simulations. For both models the symmetry-breaking states at low temperatures are described by nonzero octupole moments or third-rank spin tensor order parameters. In the case of the two-dimensional kagome antiferromagnet, a sharp crossover into a coplanar state takes place at $T_k \approx 0.004J$, which we attribute to proliferation of fractional vortices. The three-dimensional model exhibits a first-order transition at $T_c \approx 0.002J$ into a phase with critical spin correlations, which possesses a long-range order of octupole moments.

DOI: 10.1103/PhysRevB.78.094423

PACS number(s): 75.10.Hk, 75.50.Ee, 75.40.Mg

I. INTRODUCTION

A two-dimensional (2D) network of corner-sharing triangles known as the kagome lattice (Fig. 1) is a prototype of geometrical frustration. The nearest-neighbor Heisenberg antiferromagnet on such a lattice has an infinite number of spin configurations minimizing the exchange energy. Both quantum¹ and classical^{2–8} spin models on the kagome lattice have attracted significant theoretical interest in the past. Realizations of the kagome lattice topology among magnetic solids were initially rather scarce, with the prime example being $\text{SrCr}_{8-x}\text{Ga}_{4+x}\text{O}_{19}$.^{9,10} In the last few years a significant number of new magnetic compounds that are believed to be related to the kagome lattice antiferromagnet have been synthesized and studied.^{11–21} Often these materials suffer from substitutional disorder, are affected by small structural deviations from the ideal kagome network, or have extra interactions, which lift the magnetic degeneracy. Nevertheless, recent neutron-scattering experiments on powder samples of large- S kagome materials, $\text{Y}_{0.5}\text{Ca}_{0.5}\text{BaCo}_4\text{O}_7$ (Ref. 19) ($S=3/2$) and deuterium jarosite²¹ ($S=5/2$), have demonstrated remarkable similarity between the measured diffuse intensities and the Monte Carlo results for the classical model.⁷ Motivated by these two seemingly good realizations of the classical kagome antiferromagnet, we reinvestigate in the present work the finite-temperature properties of this model. In particular, we consider the angular dependence of magnetic correlations, which can be measured in neutron-diffraction experiments on single crystals.

A second source of motivation is provided by the recent discovery of a three-dimensional (3D) array of corner-sharing triangles in a spin-1/2 Mott insulator $\text{Na}_4\text{Ir}_3\text{O}_8$.²² Due to similarity with its 2D counterpart, this lattice structure has been coined a hyperkagome lattice. A network of triangles with similar topology is also known to exist in gadolinium gallium garnet, $\text{Gd}_3\text{Ga}_5\text{O}_{12}$ (Refs. 23–25) ($S=7/2$), whose enigmatic behavior attracted a lot of theoretical efforts.^{26–28} Though the magnetic properties of both systems may be quite distant from those of the nearest-neighbor classical model, in the former case due to quantum effects and in the latter material due to strong dipolar interactions, it is still important to understand the properties of the classical antiferromagnet as a starting reference point. Furthermore,

recent Monte Carlo simulations²⁹ have found evidence for an interesting low-temperature phase transition for the hyperkagome antiferromagnet.

The classical ground states of the Heisenberg kagome lattice antiferromagnet are derived from the block representation of the spin Hamiltonian

$$\hat{\mathcal{H}} = J \sum_{\langle ij \rangle} \mathbf{S}_i \cdot \mathbf{S}_j = \frac{J}{2} \sum_{\Delta} (\mathbf{S}_1 + \mathbf{S}_2 + \mathbf{S}_3)_{\Delta}^2 + \text{const.} \quad (1)$$

The energy is minimized by any spin configuration, which has $\mathbf{S}_{\Delta} = 0$ for every triangular plaquette. This classical constraint is satisfied for infinitely many configurations including planar and nonplanar states. Chalker *et al.*² argued that coplanar spin states are selected by thermal fluctuations via the order by disorder effect. They also related an asymptotic selection of the spin plane with development of the nematic order^{30,31} in spin chiralities defined as

$$\boldsymbol{\kappa} = \frac{2}{3\sqrt{3}} (\mathbf{S}_1 \times \mathbf{S}_2 + \mathbf{S}_2 \times \mathbf{S}_3 + \mathbf{S}_3 \times \mathbf{S}_1) \quad (2)$$

for each triangular plaquette. The published Monte Carlo data seem to confirm this prediction^{2,7} and the corresponding point of view prevails now in the literature on frustrated magnets.

Below we present arguments that such a description is *incomplete* and the low-temperature state of the classical

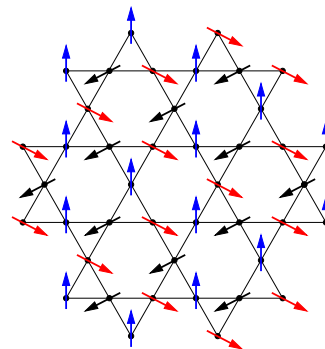


FIG. 1. (Color online) Section of the kagome lattice with spins in the fully ordered $\sqrt{3} \times \sqrt{3}$ structure.

kagome antiferromagnet should be described by a third-rank tensor or octupolar order parameter. Such a proposal was first put forward a long time ago,^{5,6,8} though no numerical results were presented to substantiate this idea. The difference between the broken symmetries for the two types of order parameters is important for topological classification of point defects in the kagome antiferromagnet. Topologically stable defects or vortices play a significant role in low-temperature transformations of 2D geometrically frustrated magnets and may lead to topological phase transitions³² and/or to an unconventional spin-glass behavior.^{5,6} The analytic consideration is supported in the following by extensive Monte Carlo simulations.

The paper is organized as follows: In Sec. II the possible tensor order parameters are considered for magnetically disordered spin systems and the presence of fractional vortices is emphasized in the case of the classical kagome antiferromagnet. Section III is devoted to Monte Carlo results for the 2D kagome antiferromagnet. In particular, the specific heat exhibits a sharp kink, which signifies formation of the coplanar spin state. In Sec. IV we investigate the behavior of the 3D kagome antiferromagnet and find that it shows a fluctuation-driven first-order transition. The low-temperature phase possesses no long-range antiferromagnetic correlations and is described instead by an octupolar order parameter.

II. SPIN TENSOR ORDER PARAMETERS

A. Symmetry analysis

Let us first recall the arguments for the order by disorder effect in the kagome antiferromagnet.^{2,4,5} Similar discussion for the hyperkagome antiferromagnet is postponed until Sec. IV. The classical constraint $\mathbf{S}_\Delta=0$ for one triangular plaquette is satisfied by a 120° spin structure. Once the orientation of the three sublattices is chosen for the first plaquette, all lowest-energy coplanar configurations can be identified with the ground states of the three-state Potts antiferromagnet or, equivalently, with coloring all sites of the kagome lattice into three colors, such that no two neighboring sites have the same color. There are $1.134 \cdot 71^N$ such states with N as the number of lattice sites.³³ The manifold of coplanar states contains two simple periodic structures: the $q=0$ state, in which all triangles pointing up (Δ) or down (∇) are in the same state, and the $\sqrt{3} \times \sqrt{3}$ structure, which is shown in Fig. 1 and is described by the wave vector $\mathbf{Q}=(4\pi/3a, 0)$, a being the lattice constant. The $q=0$ state has the same chiralities for up and down triangles, while in the $\sqrt{3} \times \sqrt{3}$ structure chiralities alternate between Δ and ∇ plaquettes.

Nonplanar states are constructed from planar configurations by identifying various closed or open two-color lines. In the $\sqrt{3} \times \sqrt{3}$ state, these are represented by hexagonal loops; see Fig. 1. Nearest neighbors off such a line are necessarily spins of the third color. Spins on the line can be continuously rotated about the direction determined by the third sublattice. The obtained spin fold (also called weather-vane mode) retains the 120° spin orientation and costs, therefore, no energy. Rotation by π returns spins back into a single plane, creating a new coplanar state.

The harmonic analysis^{2,5} indicates that coplanar states are selected at low temperatures because they have the largest number of soft excitations. The harmonic excitation spectra are identical for all coplanar configurations. Hence, selection of a specific translational pattern, if any, occurs due to weaker nonlinear effects. Therefore, there should be a range of temperatures where selection of the spin plane is not accompanied by a wave-vector selection. The heat capacity in this regime is equal to $C=11/12$ per spin.² The spin plane is specified by its normal [Eq. (2)], which for a general chirality-disordered coplanar state selects a line without direction. The corresponding order parameter is a second-rank traceless tensor:^{30,31}

$$Q_\kappa^{\alpha\beta} = \frac{1}{N_\Delta} \sum_p \left(\kappa_p^\alpha \kappa_p^\beta - \frac{1}{3} \kappa_p^2 \delta_{\alpha\beta} \right), \quad (3)$$

where the summation extends over all triangular plaquettes. A simpler form of the nematic order parameter can be constructed as a sum of on-site quadrupole moments:

$$Q^{\alpha\beta} = \frac{1}{N} \sum_i \left(S_i^\alpha S_i^\beta - \frac{1}{3} \delta_{\alpha\beta} \right). \quad (4)$$

The two order parameters [Eqs. (3) and (4)] describe the same type of broken symmetry and it is only a matter of convenience to choose one of them.

This is not, however, the end of the story. The coplanar states break, in addition, the spin-rotational symmetry inside the plane: At large distances spins do not follow any specific translational pattern but still are chosen from the initial sublattice triad. The ground states of the XY kagome antiferromagnet with planar spins $\mathbf{S}_j=(\cos \theta_j, \sin \theta_j)$ have a long-range order in $w_j=\exp(3i\theta_j)$.⁴ Generalization to Heisenberg spins is given by an on-site octupole moment expressed as a symmetric third-rank tensor,

$$T_i^{\alpha\beta\gamma} = S_i^\alpha S_i^\beta S_i^\gamma - \frac{1}{5} S_i^\alpha \delta_{\beta\gamma} - \frac{1}{5} S_i^\beta \delta_{\alpha\gamma} - \frac{1}{5} S_i^\gamma \delta_{\alpha\beta}, \quad (5)$$

with vanishing trace over any pair of indexes. The uniform long-range order of such octupoles is described by nonzero values of

$$T^{\alpha\beta\gamma} = \frac{1}{N} \sum_i \langle T_i^{\alpha\beta\gamma} \rangle, \quad (6)$$

where $\langle \dots \rangle$ denotes thermodynamic averaging. The tensor $T^{\alpha\beta\gamma}$ has in total seven independent components, as follows from its symmetry and tracelessness. Note that a similar duality in the choice between the two tensor order parameters exists for liquid crystals consisting of bent-core molecules.^{34,35} A complete characterization of the orientational order in such systems requires definition of a third-rank tensor order parameter in addition to the more familiar nematic tensor. Different forms of third-rank spin tensors have been discussed in the literature.^{5,8,36,37} For classical spins all of them are equivalent to Eq. (5), the latter form being more convenient for numerical simulations.

The order parameters $T^{\alpha\beta\gamma}$ and $Q^{\alpha\beta}$ transform according to different irreducible representations of the rotation group

SO(3) corresponding to the angular momenta $l=3$ and $l=2$, respectively. This does not mean, however, that octupole and quadrupole moments cannot coexist below the critical point. The two order parameters are coupled by a rotationally invariant term in the free-energy functional

$$\Delta\mathcal{F}_{QT} \approx Q^{\alpha\beta}T^{\alpha\mu\nu}T^{\beta\mu\nu}. \quad (7)$$

Due to time-reversal symmetry, the octupole moment has zero average value in the nematic phase. In contrast, an instability driven by $T^{\alpha\beta\gamma}$ also induces a nonvanishing quadrupolar tensor unless $\langle T^{\alpha\mu\nu}T^{\beta\mu\nu} \rangle = \delta_{\alpha\beta}$. Since the ensemble of coplanar state is described by nonzero values of both tensors, the primary order parameter for the kagome antiferromagnet is the octupole moment [Eq. (6)]. The quadrupole moment in this case is only a secondary order parameter. In the nomenclature of phase transition theory, the low- T state of the kagome antiferromagnet can be called ‘‘improper spin nematic.’’ Numerical data in support of the above conclusion are presented in Sec. III B.

Possible symmetries of a uniform octupolar state are deduced by minimizing the Landau free-energy functional:

$$\mathcal{F}_T = rT^{\alpha\beta\gamma}T^{\alpha\beta\gamma} + u(T^{\alpha\beta\gamma}T^{\alpha\beta\gamma})^2 + vT^{\alpha\beta\gamma}T^{\alpha\delta\mu}T^{\beta\delta\nu}T^{\gamma\mu\nu}. \quad (8)$$

For $v > 0$, the stable phase has D_3 symmetry, whereas for $v < 0$, it is invariant under tetrahedral point group.^{34,35} The low-temperature state of the kagome antiferromagnet is, naturally, identified with the D_3 -symmetric ‘‘triatric’’ state: D_3 spin rotations permute three spin sublattices and transform one translationally disordered coplanar state into another one from the same ensemble. The spin tensor for the triatic state can be parametrized as

$$T^{\alpha\beta\gamma} \propto (l^\alpha l^\beta l^\gamma - l^\alpha m^\beta m^\gamma - m^\alpha l^\beta m^\gamma - m^\alpha m^\beta l^\gamma) \quad (9)$$

with two orthogonal unit vectors \mathbf{l} and \mathbf{m} lying in the spin plane. The ‘‘tetrahedric’’ phase ($v < 0$) is not realized in the present spin model. Note that interaction term (7) vanishes in the tetrahedric state. Hence stabilization of the triatic phase can be ascribed to a strong coupling between the octupolar and the nematic order parameters in the kagome antiferromagnet.

For 2D Heisenberg antiferromagnets the true long-range order is impossible at any finite temperature. The above discussion applies in this situation to a symmetry of spin correlations at short distances. For distances larger than the correlation length, $r > \xi$, order parameters (3)–(6) vanish and one has to consider instead the generalized susceptibilities $\chi_V = N\langle V^2 \rangle / T$, with $V = Q^{\alpha\beta}$ and $T^{\alpha\beta\gamma}$. The lattice-averaged squares of the two spin tensors, which are directly measured in Monte Carlo simulations, are

$$\langle Q^{\alpha\beta} \rangle^2 = \frac{1}{N^2} \sum_{ij} \left[\langle (\mathbf{S}_i \cdot \mathbf{S}_j)^2 \rangle - \frac{1}{3} \right] \quad (10)$$

and

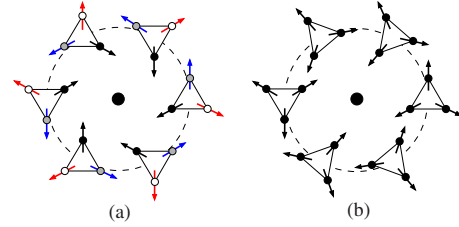


FIG. 2. (Color online) Stable topological defects in noncollinear Heisenberg antiferromagnets. The three-sublattice 120° spin structure is locally represented by orientations of equilateral triangles. Two examples of the spin texture correspond to (a) Z_2 vortex in the triangular lattice antiferromagnet with the winding number $n=+1$ and (b) fractional vortex in the kagome antiferromagnet with $n=+1/3$.

$$\langle T^{\alpha\beta\gamma} \rangle^2 = \frac{1}{N^2} \sum_{ij} \left[\langle (\mathbf{S}_i \cdot \mathbf{S}_j)^3 \rangle - \frac{3}{5} \langle \mathbf{S}_i \cdot \mathbf{S}_j \rangle \right]. \quad (11)$$

At zero temperature, in the fully ordered triatic phase (the ground state of the three-state Potts model), the above expressions yield the following limiting values: $\langle \langle Q^{\alpha\beta} \rangle^2 \rangle = 1/6$ and $\langle \langle T^{\alpha\beta\gamma} \rangle^2 \rangle = 1/4$.

B. Topological analysis

A state with ordered octupole moments also exhibits non-trivial topological properties.³⁸ The order-parameter space of the kagome antiferromagnet is obtained as a coset space $R = \text{SO}(3)/D_3$. It has the non-Abelian homotopy group $\pi_1(R) = D_6$. The symmetry of the octupolar phase allows, therefore, the presence of stable topological defects. It is instructive to compare the topological properties of the kagome antiferromagnet with those of its weakly frustrated counterpart, the triangular lattice antiferromagnet. The latter spin system is conventionally ordered into the 120° spin state, which breaks completely the rotational symmetry. The long-range translational order leaves no discrete symmetries of the spin structure. As a result, the degeneracy space of the order parameter is $R = \text{SO}(3)$ and point defects are Z_2 vortices: $\pi_1[\text{SO}(3)] = \mathbb{Z}_2$.³² A possible realization of Z_2 vortex is shown in Fig. 2(a) and corresponds to a pattern with all spins lying on a common plane and performing a 2π rotation around the vortex center. Equivalently, it can be represented as rotation of equilateral triangles with distinguishable vertices.

For a coplanar state of the kagome antiferromagnet, spin folds permute three spin sublattices and the slow spatial variations of the magnetic order parameter are represented by a texture of equilateral triangles with equivalent vertices. An elementary point defect is, consequently, a fractional vortex with $\pm 2\pi/3$ rotation around the vortex core; see Fig. 2(b). These $1/3$ vortices are known to reduce substantially the Kosterlitz-Thouless transition temperature in the XY kagome antiferromagnet.^{39,40}

In Heisenberg magnets topological defects may have a more complicated nonplanar structure. Simple hydrodynamic arguments suggest that the nonplanar Z_2 vortex in the triangular antiferromagnet has a lower energy compared to the planar vortex in Fig. 2(a).³² The same line of arguments ap-

plies also to defects in the kagome antiferromagnet. In addition, the hydrodynamic energy of $1/3$ vortices is further reduced by a factor of $1/9$ due to the smaller phase winding. As a result, entropic generation of fractional vortices in the kagome antiferromagnet starts at significantly lower temperatures than a similar effect for Z_2 vortices in the triangular antiferromagnet. A possible role of the non-Abelian topological defects in the kagome antiferromagnet was brought to attention in Ref. 5 and will be further discussed in Sec. III B.

III. KAGOME ANTIFERROMAGNET

A. Monte Carlo algorithm

The published Monte Carlo data for the nearest-neighbor Heisenberg antiferromagnet on the kagome lattice were performed on relatively small clusters of $N=3L^2$ spins with $L \leq 24$ ($N \leq 1728$).^{2,4,7} Numerical results in the present work have been obtained for a substantially wider range of lattices with $L=12-72$. The standard Metropolis algorithm has been adopted. A site on a periodic cluster is randomly picked up and a new orientation of spin is chosen. The new direction is accepted according to the Metropolis rejection scheme. To increase acceptance rate a maximum variation $\Delta S^z = T$ on a z component of spin in the local coordinate frame is imposed at low temperatures. In this way the acceptance rate stays close to 50% in the whole temperature range. A sweep over the lattice in which on average every spin is attempted to move corresponds to one Monte Carlo (MC) step.

For the Heisenberg kagome antiferromagnet the slowing down develops into a serious problem at low temperatures $T/J < 0.01$. The autocorrelation time can be further reduced by using the microcanonical over-relaxation algorithm.⁴¹ Generally, for Heisenberg models the over-relaxation move consists in successive rotations of spins around their respective local field by an arbitrary angle such that the total energy remains unchanged. The simplest and most efficient realization corresponds to a π rotation, i.e., flipping a spin to the most distant direction from the initial one.⁴² Implementation of such a spin move requires neither generation of random numbers nor calculation of trigonometric functions, which saves significant operation time. Lattice scans can be performed with random or sequential selection of spins. We find that collective motion of spins is generated more efficiently in the latter procedure, yielding faster decorrelation. Finally, one hybrid MC step consists of one canonical MC step followed by a few microcanonical nonrandom updates. Such deterministic reshuffling of spins is essential for reducing autocorrelation times at low temperatures. Typically we use between three and ten over-relaxation updates per one MC step depending on cluster size.

Each finite cluster was initiated with a random spin configuration and gradually cooled to the lowest temperature $T/J=10^{-4}$. At every temperature 5×10^4 hybrid MC steps were allowed for equilibration, which were followed by measurements ($\sim 5 \times 10^5$) performed in intervals of five hybrid MC steps. In addition, all measured quantities have been averaged over 20–50 cooling runs, starting from different random configurations. This further helps to overcome a freezing problem and also provides an unbiased estimate of

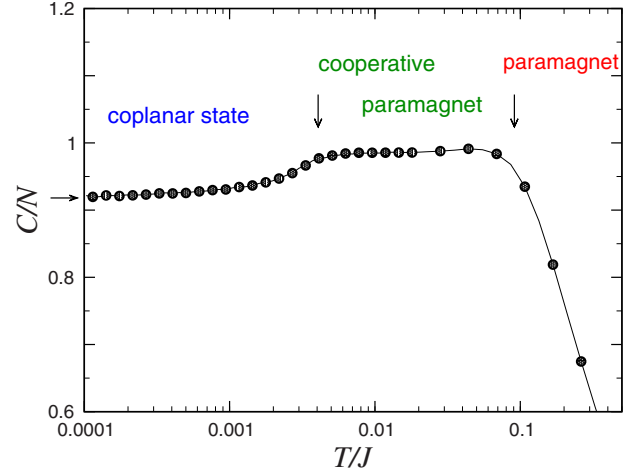


FIG. 3. (Color online) Temperature dependence of the specific heat for a kagome lattice cluster with $L=36$. The horizontal arrow denotes the value $C/N = \frac{11}{12}$. The two vertical arrows indicate boundaries between three different regimes.

the statistical errors. Unless otherwise specified, the error bars do not exceed the symbol sizes. Special checks have been performed to verify that the hybrid MC algorithm works efficiently in the relevant temperature range when instead of gradual cooling we start from either a random spin configuration or the ordered $\sqrt{3} \times \sqrt{3}$ structure. Full thermal equilibration of the $q=0$ ground state was achieved only for $T/J \geq 0.002$, which is still significantly better than in the previous studies.^{2,7}

B. Macroscopic properties

Let us begin with the heat capacity, which has been computed from fluctuations of the internal energy, $C = (\langle E^2 \rangle - \langle E \rangle^2) / T^2$. The temperature dependence of $C(T)$ on a linear-logarithmic scale is shown in Fig. 3 for a cluster with $L=36$. One can clearly distinguish three different regimes for the specific heat with the two crossover points indicated by vertical arrows. The high-temperature regime $T/J \geq 0.1$ corresponds to a paramagnetic phase with only weak correlations between neighboring spins. In the intermediate regime $0.005 \leq T/J \leq 0.1$, the internal energy reaches its classical minimum value $E/N = -J$ up to a small contribution from thermal fluctuations. Spins on triangular plaquettes become strongly correlated and satisfy approximately the constraint condition $\mathbf{S}_{\Delta} = 0$. This regime is commonly known as a classical spin liquid or a cooperative paramagnet.⁴³ The specific heat in the cooperative paramagnetic state remains close to $C/N=1$, which reflects the absence of soft modes in the excitation spectrum.

Selection of smooth, locally coplanar spin configurations takes place at $T/J \leq 0.005$ as indicated by a reduced specific heat. The probability distribution peaks in the vicinity of coplanar ground states, which have one zero (anharmonic) mode for every hexagon. The limiting value $C/N|_{T \rightarrow 0}$ coincides quite accurately with $11/12 = 0.916\dots$ predicted by the mode counting analysis.²

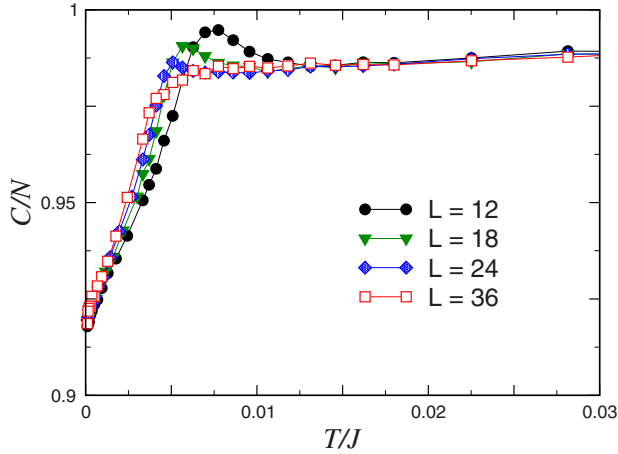


FIG. 4. (Color online) Finite-size behavior of the specific heat in the low-temperature region.

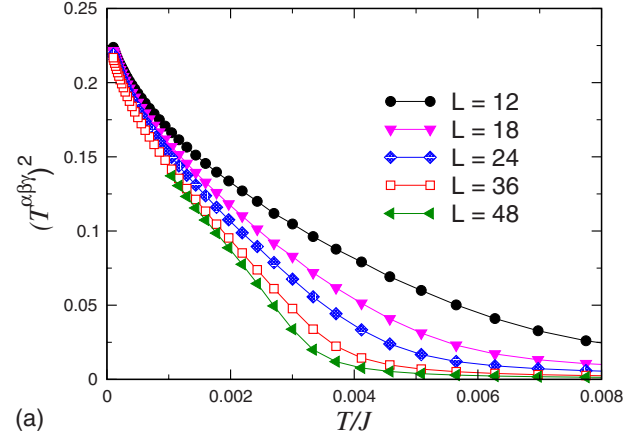
The enlarged low-temperature part of $C(T)$ is shown in Fig. 4 for several cluster sizes. Two features are noteworthy. First, the crossover between a planar spin state and a cooperative paramagnet corresponds to a rather sharp kink in $C(T)$ at around $T_k/J = 0.004 \pm 0.0005$. At $T < T_k$ the specific heat grows linearly with temperature, which can be accounted for by interaction between the spin waves. Second, the specific heat exhibits a peculiar finite-size behavior in the vicinity of the kink point, showing a rounded peak on small clusters, which disappears for $L \geq 30$ with no significant finite-size corrections afterward.

The temperature dependence of the mean square of the octupole moment is shown in Fig. 5(a). Large clusters exhibit a clear enhancement of the order parameter below $T_k/J \approx 0.004$, which coincides with a kink position in the specific heat. At low temperatures, $\langle (T^{\alpha\beta\gamma})^2 \rangle$ approaches 1/4, which is the limiting value for the fully ordered coplanar phase. The octupolar susceptibility

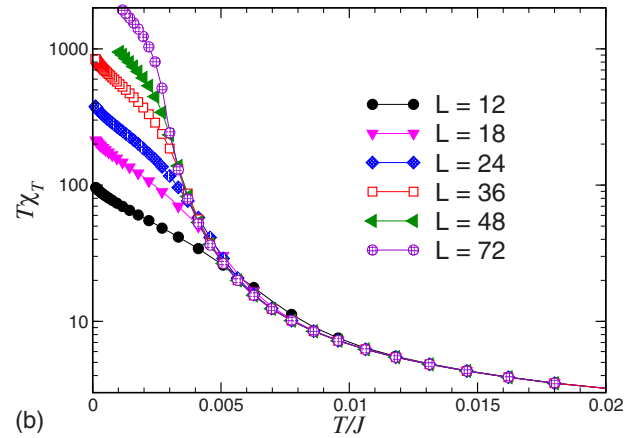
$$\chi_T = \frac{1}{TN} \sum_{i,j} \langle T_i^{\alpha\beta\gamma} T_j^{\alpha\beta\gamma} \rangle \quad (12)$$

is presented in Fig. 5(b). For each cluster there is an inflection point T_L^* below which the correlation length ξ_T becomes on the order of the linear lattice size, $\xi_T \sim L$, and the susceptibility begins to exhibit finite-size effects. The lattice-independent part of χ_T diverges as $T \rightarrow 0$, signaling a long-range-ordered state at $T=0$. The fast increase in $\chi_T(T)$ at low temperatures is consistent with a typical divergence $\chi_T(T) \approx AT^n \exp(B/T)$ found from the nonlinear sigma model mapping,⁴⁴ though no specific predictions for A , B , and n exists for the kagome antiferromagnet. Note that a rapid crossover in the behavior of $\chi_T(T)$ takes place in the vicinity of $T/J \sim 0.005$.

The behaviors of the two order parameters $T^{\alpha\beta\gamma}$ and $Q^{\alpha\beta}$ are compared in Fig. 6. The octupole moment shows a faster growth with decreasing temperature, which would correspond to a larger exponent if a second-order transition is assigned to T_k . Figure 6 illustrates our previous conclusion that the octupolar order parameter drives the low-temperature transformation in the kagome antiferromagnet.



(a)



(b)

FIG. 5. (Color online) Temperature dependences of (a) the octupolar order parameter and (b) the corresponding susceptibility for different cluster sizes.

Finally, we investigate the elastic properties of the kagome antiferromagnet by computing the temperature dependence of the spin stiffness. The spin stiffness ρ_s is defined as the second derivative of the free energy with respect to weak nonuniform twist of spins performed about a certain direction α in spin space:

$$\Delta F = \frac{1}{2} \int d^2r \rho_s [\nabla \theta^\alpha(\mathbf{r})]^2. \quad (13)$$

Substituting $\theta_i^\alpha = \delta\theta(\hat{\mathbf{e}} \cdot \mathbf{r}_i)$ for the twist angle and taking the limit $\delta\theta \rightarrow 0$, we obtain the following expression after proper symmetrization and normalization per unit area:

$$\rho_s = -\frac{\sqrt{3}}{2N} \left\{ \frac{1}{3} \langle E \rangle + \frac{J^2}{T} \left\langle \left[\sum_{\langle ij \rangle} (\mathbf{S}_i \times \mathbf{S}_j)^\alpha (\hat{\mathbf{e}} \cdot \delta_{ij}) \right]^2 \right\rangle \right\}, \quad (14)$$

where $\langle E \rangle$ is the internal energy and $\hat{\mathbf{e}}$ is an arbitrary unit vector on the lattice plane.

Numerical results for $\rho_s(T)$ are presented in Fig. 7 for three system sizes. The spin stiffness vanishes at temperatures above $T/J \sim 0.005$. This further supports identification of the intermediate phase at $0.005 \leq T/J \leq 0.1$ with the cooperative paramagnet, which has well developed local spin cor-

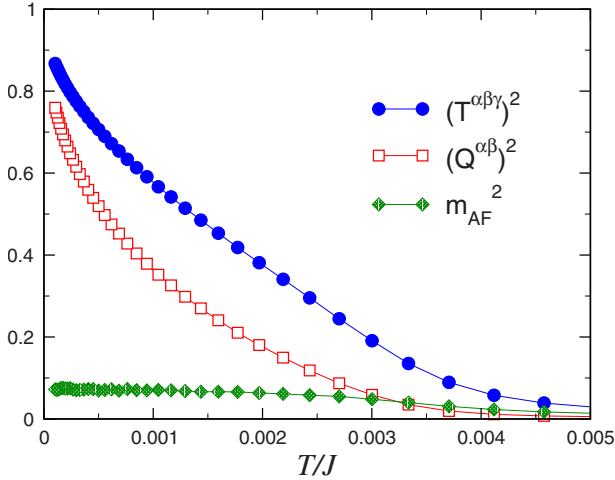


FIG. 6. (Color online) Temperature dependence of the three order parameters normalized to their respective values in the fully ordered state. Numerical data are for a cluster with $L=36$.

relations but exhibits zero response to long-wavelength perturbations. The spin rigidity starts to increase at $T/J \leq 0.004$ simultaneously with the development of short-range octupolar correlations. Finite-size scaling in the low-temperature regime still yields $\rho_s=0$ as it should be for a 2D Heisenberg spin system.

The origin of the sharp crossover in various properties of the kagome antiferromagnet at $T \sim T_k \approx 0.004J$ deserves special attention. The possible phase transition in 2D continuous non-Abelian models driven by nontrivial topological defects has been discussed in the context of two different physical applications. The first group of works motivated by investigation of liquid crystals has studied the RP^2 model in two dimensions, which in the spin language corresponds to a model of three-component spins on a square lattice coupled with ferroquadratic exchange.^{45–48} The order-parameter space is the projective sphere $RP^2 = S^2/Z_2$ with the first homotopy group $\pi_1(RP^2) = Z_2$. The topological defects in this context are called disclinations. Independently, the role of topological defects was emphasized for 2D noncollinear Heisenberg antiferromagnets.^{32,49–53} The order-parameter space is $SO(3) = S^3/Z_2$ in this case and the fundamental group is the same, $\pi_1[SO(3)] = Z_2$. For both types of models a straightforward generalization of the Kosterlitz-Thouless scenario suggests that topologically stable Z_2 vortices are bound in pairs for $T < T_v$ and become free in the high-temperature phase.^{32,45}

Kawamura and Miyashita³² investigated numerically the Heisenberg antiferromagnet on a triangular lattice and found evidence for the vortex unbinding transition at $T_v \sim 0.3J$. The heat capacity exhibits a weak maximum in the vicinity of T_v . The main difference with the standard Kosterlitz-Thouless transition in planar spin systems is that the correlation length remains finite both above and below T_v . This leads to a small finite density of free defects in the low-temperature phase. The low- and the high-temperature phases are still distinguished by an asymptotic behavior of the vorticity on a large closed contour: The vorticity function changes from the perimeter law at $T < T_v$ to the area law at $T > T_v$.^{32,50,52} The

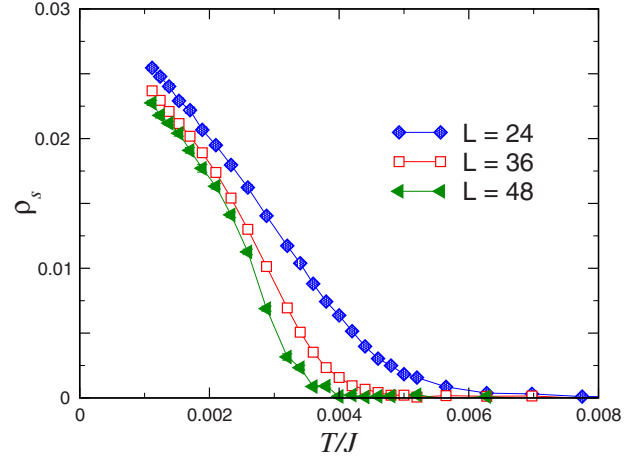


FIG. 7. (Color online) Spin stiffness of the kagome antiferromagnet for different cluster sizes.

renormalization-group analysis becomes, however, notoriously difficult since in this case it must include simultaneously spin waves and Z_2 vortices. The precise form of a singularity in the thermodynamic potential at such a topological transition remains unknown up to now.⁵¹

The topological properties of the kagome antiferromagnet suggest a natural interpretation of the observed crossover in terms of unbinding of fractional vortices. It may also provide another example of topological transition in 2D Heisenberg antiferromagnets. The kink anomaly in $C(T)$ is consistent with a cusp-type singularity in the specific heat found at the topological transition for the RP^2 model⁴⁷ and for the triangular antiferromagnet.³² The behavior of the spin stiffness also agrees with the defect unbinding scenario. Similar to the Kosterlitz-Thouless transition, free topological defects are responsible for vanishing $\rho_s=0$ above the crossover point, whereas a much slower decrease in ρ_s with the system size at low temperatures is determined by spin-wave excitations. Further numerical studies, which directly measure the density of fractional vortices and the corresponding vorticity function, are necessary to clarify the above conjecture of topological transition in the kagome antiferromagnet.

C. Spin correlations

The high-temperature series expansion for the kagome antiferromagnet³ finds that the maximum in the momentum-dependent susceptibility corresponds to the $\sqrt{3} \times \sqrt{3}$ spin structure. A similar conclusion has been made by Huse and Rutenberg⁴ from a different perspective: Spin correlations of the three-state Potts model are dominated by the staggered component at the wave vector of the $\sqrt{3} \times \sqrt{3}$ structure with a power-law decay $\sim r^{-4/3}$ at long distances. Such a purely entropic effect derived from the mapping to the two-component height model is related to the fact that the “flat” $\sqrt{3} \times \sqrt{3}$ structure maximizes the number of flippable loops. An enhancement of the antiferromagnetic correlations at low temperatures was also seen in the Monte Carlo simulations of the Heisenberg model.^{4,7}

We have investigated spin correlations in the kagome antiferromagnet by using the following form of the staggered magnetization:

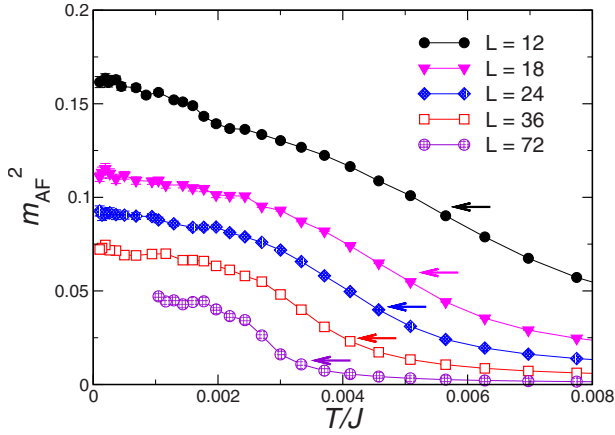


FIG. 8. (Color online) Temperature dependence of the antiferromagnetic order parameter for different cluster sizes. Horizontal arrows indicate corresponding values in the ground state of the three-state Potts model.

$$m_{\text{AF}}^2 = \frac{6}{N^2} \sum_{l,i,j} \langle \mathbf{S}_{li} \cdot \mathbf{S}_{lj} \rangle e^{i\mathbf{Q}(\mathbf{R}_i - \mathbf{R}_j)}, \quad (15)$$

where the index l numbers spins in the unit cell; i , j , and $\mathbf{R}_{i,j}$ denote the positions of the unit cell on the triangular Bravais lattice; and $\mathbf{Q} = (4\pi/3, 0)$ is the wave vector of the $\sqrt{3} \times \sqrt{3}$ structure. The lattice constant, which is twice the intersite spacing, is chosen as the length unit. The normalization factor gives $m_{\text{AF}}^2 = 1$ in the fully ordered structure. The temperature dependence of the antiferromagnetic order parameter for several lattice sizes is presented in Fig. 8. Using the loop-flip algorithm,⁴ we have also measured the antiferromagnetic order parameter for the three-state Potts antiferromagnet at $T = 0$. The corresponding values are shown in Fig. 8 by the horizontal arrows.

Spin correlations may also yield sharp signatures in the static magnetic structure factor $S(\mathbf{q})$:

$$S(\mathbf{q}) = \frac{1}{N} \sum_{i,j} \langle \mathbf{S}_i \cdot \mathbf{S}_j \rangle e^{i\mathbf{q}(\mathbf{r}_i - \mathbf{r}_j)}, \quad (16)$$

where \mathbf{r}_i is a spin position on the 2D plane. The energy integrated neutron-scattering cross section is proportional to the instantaneous spin correlator [Eq. (16)] and provides an experimental tool for its measurement. Previous numerical works on the kagome antiferromagnet have considered only the powder-averaged structure factor.^{7,21}

In the whole range of temperatures the antiferromagnetic order parameter has much smaller values than the octupole or quadrupole moments; see also Fig. 6. The enhancement of m_{AF}^2 observed at $T/J \lesssim 0.01$ on small systems^{4,7} is significantly suppressed for larger clusters. For every lattice size L there is a characteristic temperature below which the amplitude of the $\sqrt{3} \times \sqrt{3}$ correlations becomes larger than the corresponding correlations in the ground state of the three-state Potts antiferromagnet. This happens because the π -folds dressed with short-wavelength fluctuations acquire a finite linear tension, whereas loops of all lengths are flipped with equal probability in the three-state Potts model. Still, the

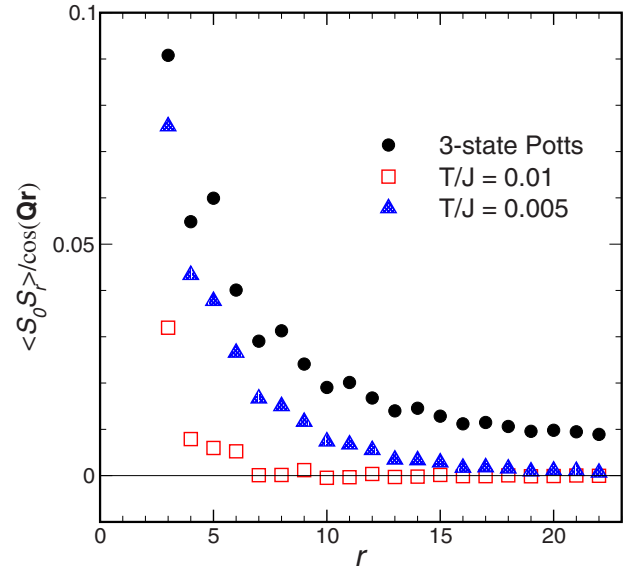


FIG. 9. (Color online) Distance dependence of spin correlators normalized to the correlations of the $\sqrt{3} \times \sqrt{3}$ structure. Correlators are measured along chain directions on the kagome lattice of linear size $L=48$. Distances are given in units of the lattice constant.

enhancement relative to the three-state Potts model is progressively shifted to lower temperatures with increasing cluster size and in the end might be a finite-size effect.

Explicit comparison of spin correlations in the Heisenberg antiferromagnet and the three-state Potts model is presented in Fig. 9 for a lattice with $L=48$. A similar plot is given in Fig. 5 of Ref. 4. Once the difference in the length scales is taken into account, the previously studied cluster corresponds to $L=12$ in our notations. At $T/J=0.005$, the spin correlations on the $L=12$ lattice approach or even exceed the amplitudes of the Potts model,⁴ which is consistent with the enhancement of the staggered magnetization shown in Fig. 8. On the other hand, the correlations for the $L=48$ cluster at the same T fall consistently below the Potts model amplitudes; see Fig. 9. There is, therefore, a fundamental difference between the low-temperature behaviors of the spin tensor order parameters and m_{AF} . While the octupole susceptibility exhibits an exponential growth as $T \rightarrow 0$, which signifies a finite value of the order parameter at $T=0$, the staggered susceptibility χ_{AF} has a much weaker increase, which for available system sizes does not exceed the corresponding values of the three-state Potts antiferromagnet.

Over the last several years it has been established that certain 2D and 3D classical spin models governed by local constraints exhibit critical behavior with power-law decay of spin correlations at long distances.^{4,54–59} A widely discussed consequence in application to the pyrochlore antiferromagnet is a “bowtie” shape of the magnetic structure factor with pinch points in certain high-symmetry directions.^{58–60} Expansion around the large- N limit for a $O(N)$ -symmetric spin model on the kagome lattice also yields a $1/r^2$ decay law for spin correlations with similar bowtie features in $S(\mathbf{q})$.⁵⁵ It is, therefore, interesting to compare magnetic intensities in the three different temperature regimes of the Heisenberg kagome antiferromagnet (Fig. 3) with the above predictions.

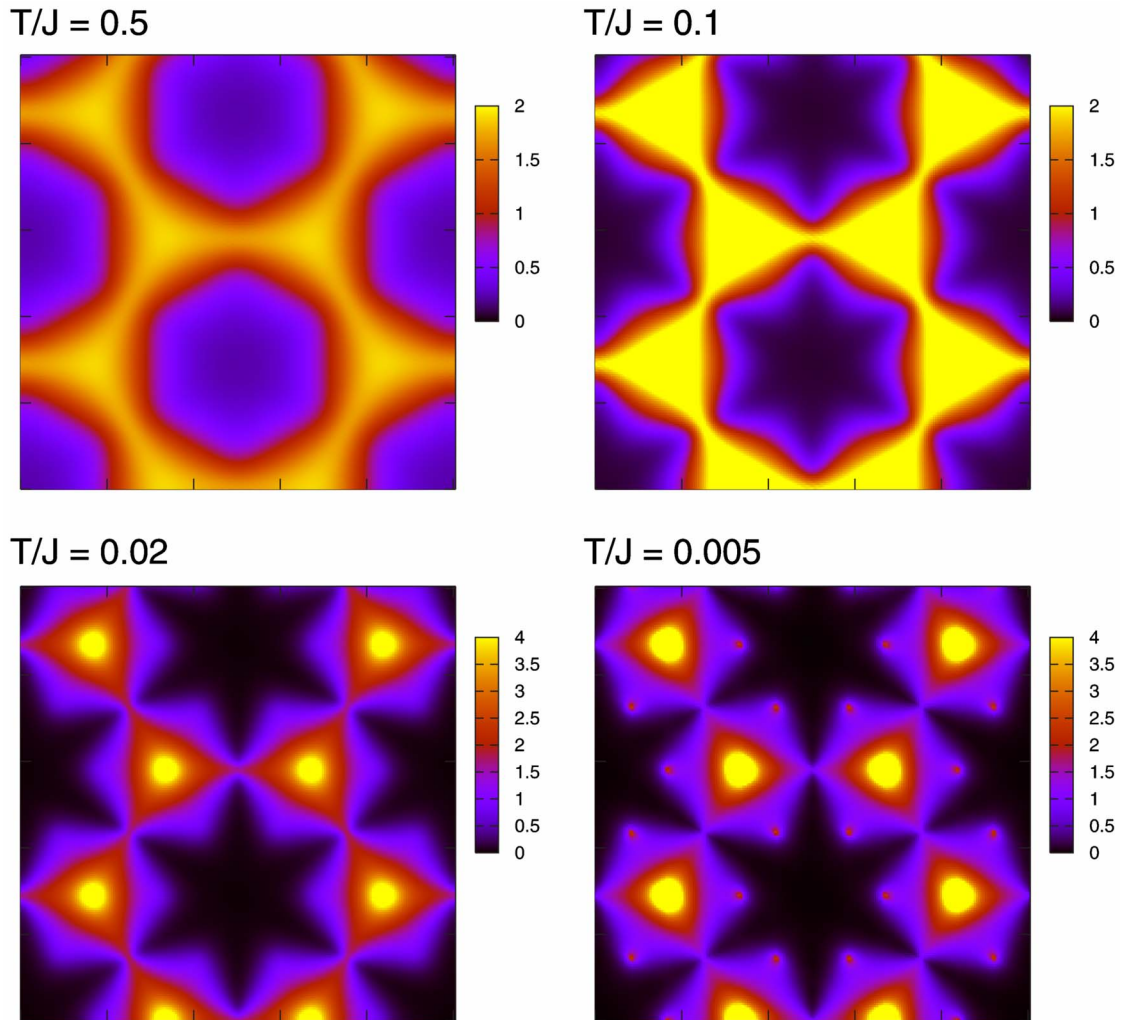


FIG. 10. (Color online) Magnetic structure factor of the kagome antiferromagnet in different temperature regimes. Region in the momentum space corresponds to $0 \leq q_{x,y} \leq 8\pi$. Note, different intensity scales for high and low temperatures.

The magnetic structure factor has been calculated for the kagome lattice cluster with $L=24$ at four different temperatures. The obtained results are shown in Fig. 10 as intensity plots on a square slice in the reciprocal space with the extension from 0 to 8π in both directions. The highest temperature $T/J=0.5$ corresponds to the paramagnetic state, where thermal fluctuations are strong and the magnetic intensity has only a broad structure in the momentum space. In the cooperative paramagnetic state at $T/J=0.1$, the pinch points develop between triangular shaped regions of strong intensity. In the vicinity of the pinch point $S(\mathbf{q})$ has a nonanalytic form due to long-distance spin-spin correlations with dipolarlike angular anisotropy.^{55,58,59} Upon cooling to a lower temperature $T/J=0.02$, the intensity is redistributed in favor of centers of the triangular regions, which correspond to $\mathbf{Q}'=2\mathbf{Q}=(8\pi/3,0)$ and equivalent wave vectors. These are not true Bragg peaks: As the spin correlations fall off as r^{-2} in this regime,⁵⁵ the peak intensity grows logarithmically with the system size. Note that peaks at the antiferromagnetic wave vector \mathbf{Q} and equivalent positions are absent.

Finally, when the coplanar correlations start to develop at $T/J=0.005$, the narrow necks loose significantly in intensity,

while new satellite peaks at $\mathbf{q}=\mathbf{Q}$ becomes noticeable. The intensity maps for $T/J=0.1$ and 0.02 most closely resemble the analytic result for $S(\mathbf{q})$ from the large- N expansion.⁵⁵ However, the magnetic intensity exhibits more structure once the order by disorder effect selects coplanar states. The development of extra diffuse peaks in the low-temperature regime is also observed in the powder-averaged structure factor.^{7,19,21} Note that the algebraic decay of spin correlations discussed above occurs at distances smaller than the correlation length. The inverse correlation length provides a natural width for all the nonanalytic features in the magnetic structure factor $S(\mathbf{q})$.

IV. HYPERKAGOME ANTIFERROMAGNET

The best known example of 3D geometrically frustrated lattice is a network of corner-sharing tetrahedra of the pyrochlore lattice; see, e.g., Ref. 61. The experimental realizations include numerous magnetic pyrochlore and spinel compounds. The only example of a 3D lattice of corner-sharing triangles was so far provided by gadolinium gallium garnet, $\text{Gd}_3\text{Ga}_5\text{O}_{12}$.^{23,24} The recent experiment has found another in-

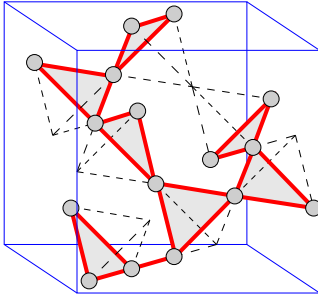


FIG. 11. (Color online) The hyperkagome lattice as a 1/4-depleted pyrochlore structure.

interesting example of a 3D triangular network of magnetic ions in $\text{Na}_4\text{Ir}_3\text{O}_8$.²² The corresponding lattice structure can be obtained by 1/4 depletion of the pyrochlore lattice such that only three out of the four vertices of each tetrahedron are occupied by magnetic ions; see Fig. 11. By analogy with the kagome lattice, this structure is called the hyperkagome lattice. It contains 12 spins in the standard cubic unit cell. The garnet lattice has, in contrast, 24 spins in its cubic unit cell and consists of two interpenetrating hyperkagome sublattices. The positions of the atoms in each garnet sublattice are different from the 1/4-depleted pyrochlore structure but the topology of the two networks remains the same. The local symmetry on magnetic sites is somewhat higher in the garnet structure containing a twofold rotational axis joining centers of adjacent triangles.

In this section we consider a classical Heisenberg antiferromagnet on the hyperkagome lattice. The limited applicability of such a model to the above two magnetic materials has been mentioned before. Still this model is quite interesting on its own, in particular, in contrast with the more familiar 2D system. The arguments given before for the infinite degeneracy of the classical ground states of the kagome antiferromagnet (Secs. I and II) are fully applicable to the 3D model and will not be repeated here. The coplanar configurations play again an important role at low temperatures. The harmonic analysis finds $N/3$ zero-energy modes for the hyperkagome antiferromagnet out from the total $2N$ modes for N classical spins.^{27,29} This yields the same limiting value for the specific heat $C/N|_{T \rightarrow 0} = 11/12$ as for the 2D model. Soft modes reside on closed loops, which pass through at least ten triangles.^{27,62}

A submanifold of coplanar configurations is again mapped to the ground states of the three-state Potts antiferromagnet on the hyperkagome lattice. The precise number of such states or, equivalently, the ways of coloring sites with three colors is not known for the 3D lattice. A local gauge representation of the classical constraint with the Maxwellian-type action predicts the dipolar form of the spin-spin correlation function.^{29,57} Performing loop-algorithm simulations in the ground-state ensemble of the Potts antiferromagnet, we indeed found a very fast decay of spin correlations consistent with an r^{-3} dependence.

The general mode counting arguments suggest the presence of the order by disorder effect for three-component spins on a lattice of corner-sharing triangles.⁶¹ Though the early numerical work found no evidence of such an effect,²⁶

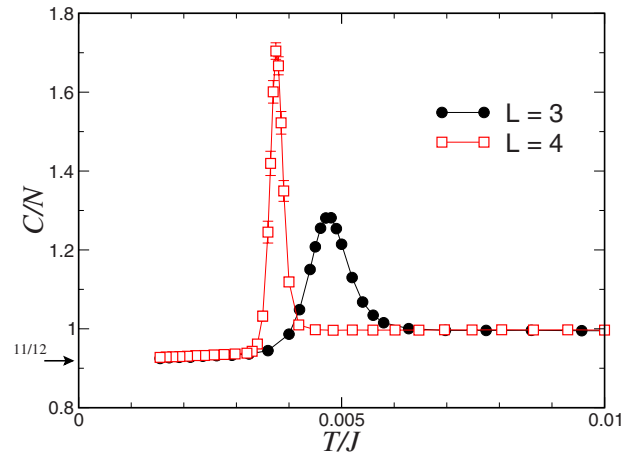


FIG. 12. (Color online) Low-temperature specific heat of the classical hyperkagome antiferromagnet.

the recent Monte Carlo study detected a first-order transition at $T/J \leq 0.004$.²⁹ The authors argued in favor of a nematic state below the transition. As we have shown in Sec. II the full symmetry-breaking pattern in the submanifold of the coplanar states is described by the octupolar order parameter. The first-order nature of the transition is not surprising in this respect as the renormalization-group analysis of Landau free-energy functional (8) finds no stable fixed-point solution below four dimensions.³⁴

To verify the formation of the octupolar ordering in the hyperkagome antiferromagnet, we have performed the classical Monte Carlo simulations on periodic clusters with $N = 12L^3$ spins and $L = 3-6$. The equilibration problem at low temperatures in three dimensions becomes much more severe compared to the 2D model. The published data²⁹ show, for example, a strong hysteresis for $L \geq 4$, which clearly indicates that large clusters fall out of equilibrium. We resort, therefore, to the exchange Monte Carlo algorithm⁶³ in conjunction with the hybrid updates described before. We use between 30 and 50 replicas depending on cluster size distributed in the temperature interval $0.001 < T/J < 0.02$. All replicas are initiated with random spin configurations, which are equilibrated for 10^6 exchange MC steps. These are followed by measurements for 5×10^5 MC steps. Finally, the results have been averaged over 20 independent runs to determine statistical errors.

The numerical data for the specific heat obtained on two smallest clusters are presented in Fig. 12. At temperatures below the anomaly, the specific heat approaches the value $C/N = 11/12$ predicted for the coplanar state by the mode counting analysis. The fast growth of the peak height is consistent with $C/N \propto L^3$ scaling expected for the first-order transition.⁶⁴

The temperature dependence of the mean square of the octupolar order parameter is shown in Fig. 13. The transition temperature for each cluster can be estimated at the mid-height of the jump. The order parameter exhibits extremely weak finite-size dependence at low temperatures, which signifies development of the true long-range octupolar ordering in this 3D spin model. Still, a certain amount of disorder in the low-temperature phase is evidenced by deviations of

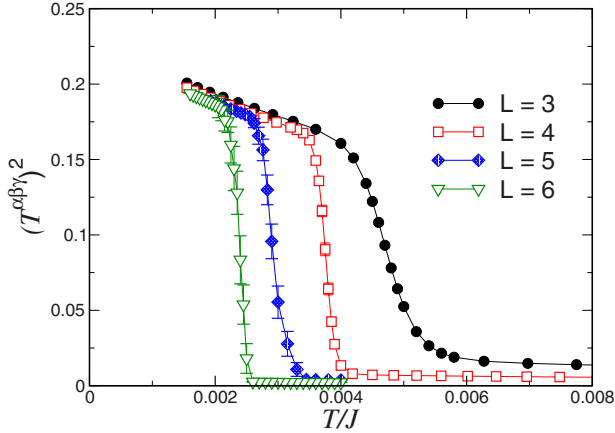


FIG. 13. (Color online) Mean square of the octupolar order parameter versus temperature for the hyperkagome antiferromagnet.

$\langle (T^{\alpha\beta\gamma})^2 \rangle$ from the limiting value of 1/4 for the fully ordered octupolar structure. A simple scaling of the transition temperature with the cluster size yields $T_c/J = 0.002 \pm 0.0003$ for the transition temperature. In order to locate more accurately the point of first-order transition, one needs to simulate bigger lattices, which appears to be a difficult task even for the exchange Monte Carlo algorithm.

In order to check a tendency to a long-range magnetic ordering below T_c at *a priori* unknown wave vector, we have calculated the angular-averaged structure factor:

$$S(q) = \frac{1}{N} \sum_j \langle \mathbf{S}_i \cdot \mathbf{S}_j \rangle \frac{\sin(q|\mathbf{r}_{ij}|)}{q|\mathbf{r}_{ij}|}. \quad (17)$$

The neutron-diffraction experiments on polycrystalline samples allow one to directly measure $S(q)$. The results for the $L=5$ cluster are presented in Fig. 14. The static structure factor $S(q)$ below T_c exhibits broad diffuse peaks with no sharp features, which could point at a long-range order. We have found only a tiny change in $S(q)$ across the first-order transition. Variation of temperature by 2 orders of magnitude

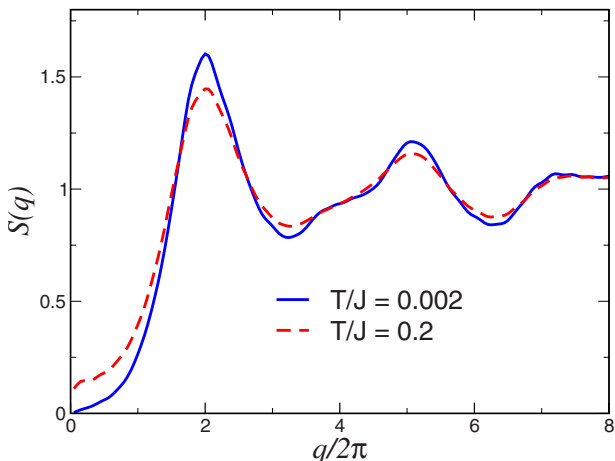


FIG. 14. (Color online) Powder-averaged magnetic structure factor for the hyperkagome antiferromagnet. Wave vectors are given in reciprocal-lattice units.

from $T/J=0.2$ to 0.002 leads only to a small increase of $\sim 15\%$ in the main peak intensity. A similar form of the diffuse structure factor at high temperatures was previously obtained in the numerical work on gadolinium gallium garnet.²⁵ The nearest-neighbor classical Heisenberg antiferromagnet on the hyperkagome lattice provides a unique example of the long-range-ordered state of magnetic octupoles with algebraically decaying spin-spin correlations.

Returning back to $\text{Na}_4\text{Ir}_3\text{O}_8$, the recent experiment²² has demonstrated the absence of magnetic ordering down to 2 K, which is significantly smaller than the scale of antiferromagnetic interactions deduced from the Curie-Weiss constant $\theta_{\text{CW}} \sim 650$ K. Such a behavior is consistent with strong geometrical frustration found for the nearest-neighbor hyperkagome antiferromagnet.^{26,29,62} It would be interesting to compare the neutron-diffraction data in the spin-liquid state of $\text{Na}_4\text{Ir}_3\text{O}_8$ with the above results for $S(q)$. This should allow one, in particular, to verify the relevance of the nearest-neighbor Heisenberg model to the real material.

V. CONCLUSIONS

We have clarified in the present work that selection of the coplanar states in the kagome antiferromagnet is properly described by the development of the octupolar (third-rank spin tensor) order parameter. Our Monte Carlo simulations yield $T_k \approx 0.004J$ for the onset of coplanar ordering, which is lower than the previous estimates.^{2,7} Furthermore, we suggest that T_k may correspond to a topological transition, which consists in unbinding of fractional vortices. Presence of these topologically stable point defects follows from the nontrivial degeneracy space of the octupolar order parameter. The antiferromagnetic $\sqrt{3} \times \sqrt{3}$ correlations are also enhanced at low temperatures, though the corresponding correlation length remains significantly shorter than the characteristic length scale for octupolar correlations. Our MC data for big lattices with $L \geq 36$ do not confirm the previously made suggestion⁴ that the asymptotic $\sqrt{3} \times \sqrt{3}$ ordering develops in the limit $T \rightarrow 0$. Precise numerical study of the lowest temperature region $T/J \leq 10^{-3}$ definitely requires simulations on clusters with $L > 72$, which is impossible without new Monte Carlo algorithms (but see also the last paragraph).

The classical hyperkagome antiferromagnet provides a unique example of the spin model with the long-range octupolar ordering. In the broken-symmetry state below a fluctuation-induced first-order transition, spin correlations remain critical with a power-law decay r^{-3} at long distances.^{29,57} It is interesting to study the phase diagram in magnetic field for this model, in particular, in relation to the experimental diagram of $\text{Gd}_3\text{Ga}_5\text{O}_{12}$, which exhibits a field-induced ordered phase.^{23–25}

Let us finish with a few comments on the possible relation of the topological transition to the spin-glass-like behavior observed in some jarosites.^{12,13} Similar to the previous numerical studies we find a very strong tendency to spin freezing once the coplanar configurations are stabilized at $T < T_u$. It is the hybrid Monte Carlo algorithm adopted in the present work, which allows one to equilibrate large spin systems at low temperatures. The spin reshuffling dynamics of the mi-

crocanonical sweeps has no simple analog in real magnetic materials. The kagome antiferromagnet will be, therefore, stuck in one of the many degenerate coplanar states with frozen structure of chirally ordered domains. Rotation of spins along spin folds is suppressed due to development of free-energy barriers of the entropic origin.^{2,5,6} Above the topological transition, when thermally excited vortices destroy the common plane and remove the entropic barriers, the single spin-flip dynamics becomes effective again. The above ideas for the unconventional spin-glass transition were pioneered by Ritchey and co-workers.^{5,6} The results of our work put emphasis on a hidden topological transition behind

a spin-glass freezing in geometrically frustrated magnets. Though the corresponding temperature scale comprises only a small fraction of θ_{CW} for the Heisenberg antiferromagnet, intrinsic XY anisotropies in real materials can significantly enhance T_v by transforming it to the Kosterlitz-Thouless transition for $1/3$ vortices.

ACKNOWLEDGMENTS

I am grateful to B. Fåk, R. Moessner, and P. Thalmeier for helpful discussions. I thank the MPI-PKS (Dresden) for the hospitality.

-
- ¹See, e.g., G. Misguich and C. Lhuillier, in *Frustrated Spin Systems*, edited by H. T. Diep (World-Scientific, Singapore, 2004).
- ²J. T. Chalker, P. C. W. Holdsworth, and E. F. Shender, *Phys. Rev. Lett.* **68**, 855 (1992).
- ³A. B. Harris, C. Kallin, and A. J. Berlinsky, *Phys. Rev. B* **45**, 2899 (1992).
- ⁴D. A. Huse and A. D. Rutenberg, *Phys. Rev. B* **45**, 7536 (1992).
- ⁵I. Ritchey, P. Chandra, and P. Coleman, *Phys. Rev. B* **47**, 15342 (1993).
- ⁶P. Chandra, P. Coleman, and I. Ritchey, *J. Phys. I* **3**, 591 (1993).
- ⁷J. N. Reimers and A. J. Berlinsky, *Phys. Rev. B* **48**, 9539 (1993).
- ⁸M. E. Zhitomirsky, *Phys. Rev. Lett.* **88**, 057204 (2002).
- ⁹X. Obradors, A. Labarta, A. Isalgue, J. Tejada, J. Rodriguez, and M. Pernet, *Solid State Commun.* **65**, 189 (1988).
- ¹⁰A. P. Ramirez, G. P. Espinosa, and A. S. Cooper, *Phys. Rev. Lett.* **64**, 2070 (1990).
- ¹¹S.-H. Lee, C. Broholm, M. F. Collins, L. Heller, A. P. Ramirez, C. Kloc, E. Bucher, R. W. Erwin, and N. Laceyvic, *Phys. Rev. B* **56**, 8091 (1997).
- ¹²A. S. Wills, A. Harrison, S. A. M. Mentnik, T. E. Masom, and Z. Tun, *Europhys. Lett.* **42**, 325 (1998).
- ¹³A. S. Wills, A. Harrison, C. Ritter, and R. I. Smith, *Phys. Rev. B* **61**, 6156 (2000).
- ¹⁴T. Inami, M. Nishiyama, S. Maegawa, and Y. Oka, *Phys. Rev. B* **61**, 12181 (2000).
- ¹⁵Z. Hiroi, M. Hanawa, N. Kobayashi, M. Nohara, H. Takagi, Y. Kato, and M. Takigawa, *J. Phys. Soc. Jpn.* **70**, 3377 (2001).
- ¹⁶D. Grohol, D. G. Nocera, and D. Papoutsakis, *Phys. Rev. B* **67**, 064401 (2003).
- ¹⁷M. P. Shores, E. A. Nytko, B. M. Barlett, and D. G. Nocera, *J. Am. Chem. Soc.* **127**, 13462 (2005).
- ¹⁸K. Matan, D. Grohol, D. G. Nocera, T. Yildirim, A. B. Harris, S. H. Lee, S. E. Nagler, and Y. S. Lee, *Phys. Rev. Lett.* **96**, 247201 (2006).
- ¹⁹W. Schweika, M. Valldor, and P. Lemmens, *Phys. Rev. Lett.* **98**, 067201 (2007).
- ²⁰P. Mendels, F. Bert, M. A. de Vries, A. Olariu, A. Harrison, F. Duc, J. C. Trombe, J. S. Lord, A. Amato, and C. Baines, *Phys. Rev. Lett.* **98**, 077204 (2007).
- ²¹B. Fåk, F. C. Coomer, A. Harrison, D. Visser, and M. E. Zhitomirsky, *Europhys. Lett.* **81**, 17006 (2008).
- ²²Y. Okamoto, M. Nohara, H. Aruga-Katori, and H. Takagi, *Phys. Rev. Lett.* **99**, 137207 (2007).
- ²³W. I. Kinney and W. P. Wolf, *J. Appl. Phys.* **50**, 2115 (1979).
- ²⁴P. Schiffer, A. P. Ramirez, D. A. Huse, and A. J. Valentino, *Phys. Rev. Lett.* **73**, 2500 (1994).
- ²⁵O. A. Petrenko, C. Ritter, M. Yethiraj, and D. McK Paul, *Phys. Rev. Lett.* **80**, 4570 (1998).
- ²⁶O. A. Petrenko and D. McK Paul, *Phys. Rev. B* **63**, 024409 (2000).
- ²⁷M. E. Zhitomirsky, *Phys. Rev. B* **67**, 104421 (2003).
- ²⁸T. Yavors'kii, M. Enjalran, and M. J. P. Gingras, *Phys. Rev. Lett.* **97**, 267203 (2006).
- ²⁹J. M. Hopkinson, S. V. Isakov, H.-Y. Kee, and Y. B. Kim, *Phys. Rev. Lett.* **99**, 037201 (2007).
- ³⁰A. F. Andreev and I. A. Grishchuk, *Zh. Eksp. Teor. Fiz.* **87**, 467 (1984) [*Sov. Phys. JETP* **60**, 267 (1984)].
- ³¹P. Chandra and P. Coleman, *Phys. Rev. Lett.* **66**, 100 (1991).
- ³²H. Kawamura and S. Miyashita, *J. Phys. Soc. Jpn.* **53**, 9 (1984); **53**, 4138 (1984).
- ³³R. J. Baxter, *J. Math. Phys.* **11**, 784 (1970).
- ³⁴L. Radzihovsky and T. C. Lubensky, *Europhys. Lett.* **54**, 206 (2001).
- ³⁵T. C. Lubensky and L. Radzihovsky, *Phys. Rev. E* **66**, 031704 (2002).
- ³⁶V. I. Marchenko, *JETP Lett.* **48**, 427 (1988).
- ³⁷T. Momoi, P. Sindzingre, and N. Shannon, *Phys. Rev. Lett.* **97**, 257204 (2006).
- ³⁸N. D. Mermin, *Rev. Mod. Phys.* **51**, 591 (1979).
- ³⁹M. S. Rzchowski, *Phys. Rev. B* **55**, 11745 (1997).
- ⁴⁰S. E. Korshunov, *Phys. Rev. B* **65**, 054416 (2002).
- ⁴¹M. Creutz, *Phys. Rev. D* **36**, 515 (1987).
- ⁴²K. Kanki, D. Loison, and K. D. Schotte, *Eur. Phys. J. B* **44**, 309 (2005).
- ⁴³J. Villain, *Z. Phys. B* **33**, 31 (1979).
- ⁴⁴P. Azaria, B. Delamotte, T. Jolicoeur, and D. Mouhanna, *Phys. Rev. B* **45**, 12612 (1992).
- ⁴⁵S. Solomon, *Phys. Lett.* **100B**, 492 (1981).
- ⁴⁶S. Solomon, Y. Stavans, and E. Domany, *Phys. Lett.* **112B**, 373 (1982).
- ⁴⁷H. Kunz and G. Zumbach, *Phys. Rev. B* **46**, 662 (1992).
- ⁴⁸A. I. Farinas Sanchez, R. Paredes, and B. Berche, *Phys. Lett. A* **308**, 461 (2003).
- ⁴⁹M. Wintel, H. U. Everts, and W. Apel, *Europhys. Lett.* **25**, 711 (1994); *Phys. Rev. B* **52**, 13480 (1995).
- ⁵⁰B. W. Southern and H. J. Xu, *Phys. Rev. B* **52**, R3836 (1995).

- ⁵¹M. Caffarel, P. Azaria, B. Delamotte, and D. Mouhanna, Phys. Rev. B **64**, 014412 (2001).
- ⁵²H. Kawamura and A. Yamamoto, J. Phys. Soc. Jpn. **76**, 073704 (2007).
- ⁵³J.-C. Domenge, C. Lhuillier, L. Messio, L. Pierre, and P. Viot, Phys. Rev. B **77**, 172413 (2008).
- ⁵⁴J. Kondev and C. L. Henley, Phys. Rev. B **52**, 6628 (1995).
- ⁵⁵D. A. Garanin and B. Canals, Phys. Rev. B **59**, 443 (1999).
- ⁵⁶R. Moessner and S. L. Sondhi, Phys. Rev. B **68**, 064411 (2003).
- ⁵⁷D. A. Huse, W. Krauth, R. Moessner, and S. L. Sondhi, Phys. Rev. Lett. **91**, 167004 (2003).
- ⁵⁸S. V. Isakov, K. Gregor, R. Moessner, and S. L. Sondhi, Phys. Rev. Lett. **93**, 167204 (2004).
- ⁵⁹C. L. Henley, Phys. Rev. B **71**, 014424 (2005).
- ⁶⁰M. P. Zinkin, M. J. Harris, and T. Zeiske, Phys. Rev. B **56**, 11786 (1997).
- ⁶¹R. Moessner and J. T. Chalker, Phys. Rev. Lett. **80**, 2929 (1998); Phys. Rev. B **58**, 12049 (1998).
- ⁶²M. J. Lawler, H.-Y. Kee, Y. B. Kim, and A. Vishwanath, Phys. Rev. Lett. **100**, 227201 (2008).
- ⁶³K. Hukushima and K. Nemoto, J. Phys. Soc. Jpn. **65**, 1604 (1996).
- ⁶⁴K. Binder and D. P. Landau, Phys. Rev. B **30**, 1477 (1984).